Theoretical estimates of the thermoelectric power factor of graphene encapsulated between 3D and 2D semiconductor and metal slabs

© S.Yu. Davydov[1], O.V. Posrednik[2]

[1] Ioffe Institute,
194021 St. Petersburg, Russia
[2] St. Petersburg State Electrotechnical University „LETI",
197022 St. Petersburg, Russia

E-mail: Sergei_Davydov@mail.ru

Received September 13, 2023
Revised December 13, 2023
Accepted December 20, 2023

The conditions of extremeness of the conductivity, the Seebeck coefficient and the thermoelectric power factor values of encapsulated graphene, considered as a functions of the chemical potential, are determined. 3D and 2D semiconductors and transition metals are considered as slabs. The use of simple models allowed us to obtain analytical results. Numerical estimates were performed for bulk Si, Ge and 16 binary III−V and II−VI compounds, six two-dimensional semiconductor transition metal dichalcagenides and all elements of the 3*d*-, 4*d*- and 5*d*-series. Recommendations of slab materials allowing to maximize thermoelectric characteristics are given. Encapsulated two-layer graphene is also briefly discussed.

Keywords: thermoelectric characteristics, encapsulated graphene, 3D semiconductors, 2D transition metal dichalcagenides, 3D and 2D transition metals.

DOI: 10.61011/SC.2023.09.57437.5558

1. Introduction

The thermoelectric power factor $PF = \sigma S^2$ is often used to characterize thermoelectric properties, where σ is electrical conductivity, S is the Seebeck coefficient. Currently, an active search is in progress for massive (3D) [1–3] (for example, PbTe, Bi_2Te_3, SnSe, CoSi, $BaPS_2$) and two-dimensional (2D) [4,5] (for example, GeP_3, SnP_3) materials for which the dimensionless product $ZT \equiv (PF/\kappa)T > 1$, where T is temperature, κ is thermal conductivity (in English-language literature ZT, and sometimes $Z = \sigma S^2/\kappa$ are called figure of merit; such terms as thermoelectric efficiency, or Ioffe criteria are used in the Russian publications). To achieve the same goal, the theory focuses on the choice of such an electron dispersion law, which corresponds to the maximum values of PF and ZT [6–10]. For example, it considers the laws of dispersion $\varepsilon_n(\mathbf{k}) \propto k^n$ $(n = 4, 6)$ where $\mathbf{k}$ is a wave vector (such zones are called „pudding-mold type bands" in English language literature) and combinations of zones $\varepsilon_n(\mathbf{k})$ with a linear Dirac spectrum. Heterocontacts such as graphene (Gr)is metal [11], Gris 2D hexagonal boron nitride(*h*-BN) [12] and Gr-semiconductor were considered with the same aim [13]. We considered the problem of encapsulated graphene (Gr) in [14] and obtained analytical expressions for the dependences of the thermoelectric power factor on the chemical potential of the system μ. As an example, numerical estimates were performed in [14] for the structure *h*-BN/Gr/*h*-BN. It has been shown that the maximum values of PF are reached when the chemical potential, remaining inside the band gap *h*-BN, approaches its edges. Here we will consider structures where 3D and 2D semiconductors Si, Ge and binary compounds III−V and II−VI and transition metals act as sheets of single-sheet graphene, the temperature gradient is directed along the graphene sheet.

In what follows, we will use the so-called adsorption approach to the problem of [15], which consists in the following. Let the encapsulated layer be described by the Green's function $g(\omega)$, where ω is an energy variable. The effect of encapsulating layers 1 and 2 is taken into account by polarization operators (or the actual energy contribution)

$$\Sigma_{1,2}(\omega) = \Lambda_{1,2}(\omega) - i\Gamma_{1,2}(\omega),$$

where $\Lambda_{1,2}(\omega)$ and $\Gamma_{1,2}(\omega)$ represent the the shift and broadening functions the electronic states of the encapsulated layer under the action of sheets 1 and 2. In this case, the Green's function of the encapsulated layer is equal to

$$G^{-1}(\omega) = g^{-1}(\omega) - \Sigma_1(\omega) - \Sigma_2(\omega).$$

$\Lambda_{1,2}(\omega)$ and $\Gamma_{1,2}(\omega)$ functions are uniquely determined by the energy densities of the states (DOS) of the sheets 1 and 2. Simple models of these densities of states lead to the fact that the functions $\Lambda_{1,2}(\omega)$ and (or) their derivatives $d\Lambda_{1,2}(\omega)/d\omega$ have divergences, which naturally manifest themselves in expressions for the characteristics σ, S and PF. Here we should focus on those features that lead to the maximum values of thermoelectric (TE) characteristics for single-layer graphene (SLG). We briefly consider the issue of encapsulated bilayer graphene (BLG) in the *Appendix*.

2. General relations

According to the Mott formula the Seebeck coefficient is equal to

$$S = -(\pi^2 k_B^2 T/3e)[d\ln\sigma(\mu, T=0)/d\mu], \quad (1)$$

where e is elementary charge, k_B is Boltzmann constant. Thus, the problem of calculating PF is reduced to determining the dependences of conductivity and its logarithmic derivative on the position of the chemical potential μ at zero temperature. We will consider single-layer graphene located between semiconductor sheets 1 and 2 with band gaps $E_{g1,2}$, the boundaries of which are $E_{C1,2}$ and $E_{V1,2}$ (edges of conduction bands and valence bands). Further, we will assume that μ is located within the resulting band gap, the boundaries of which E_C^* and E_V^* are determined by the inequality

$$E_V^* = \max\{E_{V1}, E_{V2}\} < E_C^* = \min\{E_{C1}^*, E_{V2}^*\}.$$

Interval (E_V^*, E_C^*) is defined because PF of graphene has maximum values at $\mu \to E_{V,C}^*$ precisely within the boundaries of the band gap [14]. According to [14], at $T=0$ the dimensionless static conductivity $\sigma^* \equiv \sigma/(e^2/\pi\hbar)$, where $\hbar$ is the reduced Planck's constant has the following form

$$\sigma^* = \sigma_1^* + \sigma_2^*, \ \sigma_1^* = \frac{\xi^2 F}{F^2 + 4\tilde{\mu}^2\gamma^2}, \ \sigma_2^* = \frac{\tilde{\mu}^2+\gamma^2}{2\tilde{\mu}\gamma} R, \quad (2)$$

$$R(\mu) = \arctan\frac{F}{2\gamma\mu} + \arctan\frac{\mu^2-\gamma^2}{2\gamma\mu},$$

$$F = \xi^2 + \gamma^2 - \mu^2, \ \tilde{\mu} = \mu - \overline{\Lambda}(\mu).$$

Here $\overline{\Lambda}(\mu) = \Lambda_1(\mu) + \Lambda_2(\mu)$, where $\Lambda_{1,2}(\mu)$ are SLG level shift functions caused by interaction with the sheets 1, 2; $\xi = \sqrt{2\pi\sqrt{3}t}$ is cutoff energy for the SLG spectrum; γ is broadening of SLG levels due to the intrinsic attenuation of electronic states; the energy of the Dirac point ε_D is assumed to be zero. In the same area (E_V^*, E_C^*) derivatives $d\sigma^*/d\mu = d\sigma_1^*/d\mu + d\sigma_2^*/d\mu$ equal

$$d\sigma_1^*/d\mu = -\frac{2\xi^2\tilde{\mu}C^*}{F^2 + 4\gamma^2\tilde{\mu}^2}\left(1 - 2\frac{F(F-2\gamma^2)}{F^2+4\gamma^2\mu^2}\right),$$

$$\frac{d\sigma_2^*}{d\mu} = \frac{\mu^2-\gamma^2}{2\gamma\mu^2} CR + \frac{\mu^2+\gamma^2}{2\gamma\mu}\frac{dR}{d\mu}, \quad (3)$$

where

$$\frac{dR}{d\mu} = -4\gamma CD, \quad C = 1 - d\overline{\Lambda}/d\mu,$$

$$D = \left(\frac{\xi^2+\gamma^2}{F^2+4\gamma^2\tilde{\mu}^2} - \frac{1}{2(\mu^2+\gamma^2)}\right). \quad (4)$$

In the [14] analyzes the dependencies $\sigma^*(\mu)$

$$L(\mu) = d\ln\sigma^*/d\mu \propto S$$

and

$$PF^*(\mu) = (\sigma^*)^{-1}(d\sigma^*/d\mu)^2 \propto \sigma S^2$$

(where the function $PF^*(\mu)$ is denoted as $Z^*(\mu)$). The paper also discusses the extremums of the functions $L(\mu)$ and $PF^*(\mu)$ the positions of which $\pm\mu_{ext}^L$ and $\pm\mu_{ext}^{Z^*}$ are determined respectively from equations

$$\sigma^*(d^2\sigma^*/d\mu^2) = (d\sigma^*/d\mu)^2$$

and

$$2(d^2\sigma^*/d\mu^2) = (d\sigma^2/d\mu)^2.$$

Here, however, we do not provide the corresponding cumbersome formulas. It is necessary to set the density of states of semiconductors (DOSs) of sheets 1 and 2 and the corresponding shift and broadening functions to study specific structures.

3. 3D sheets

3.1. Semiconductor sheets

We use the [16] model, according to which the DOS of the semiconductor $\rho_{sc}(\omega)$ can be represented as follows [17]:

$$\rho_{sc}(\Omega) = \begin{cases} A_C\sqrt{\Omega - E_g/2}, & E_g/2 < \Omega \le W_C + E_g/2, \\ A_V\sqrt{-\Omega - E_g/2}, & -W_V - E_g/2 \le \Omega < -E_g/2, \\ 0, & |\Omega| \le E_g/2, \ |\Omega| > W_{C,V} + E_g/2. \end{cases} \quad (5)$$

Here $\Omega = \omega - \omega_0$, where ω_0 is the energy of the center of the band gap relative to the Dirac point; $A_{C,V}$ are coefficients, $W_{C(V)}$ is the width of the conduction band (valence band). The parameters $A_{C,V}$ and $W_{C,V}$ are related by the ratio $A_{C,V}W_{C,V}^{3/2} = 6$ [17]. Further, for simplicity, let's put $A_C = A_V = A$, $W_C = W_V = W$. Then, we obtain for the shift function

$$\Lambda(\Omega) = f_-(\Omega) - f_+(\Omega), \quad (6)$$

where

$$f_\pm(\Omega) = 2AV^2 r_\pm(\Omega)\arctan\left(\sqrt{W}/r_\pm(\Omega)\right),$$

$$r_\pm(\Omega) = \sqrt{\pm\Omega + E_g/2}$$

and V is the matrix element of the interaction of the plate with graphene. Thus,

$$\Lambda_{max} \equiv |\Lambda(\pm E_g/2)| = 2AV^2\sqrt{E_g}\arctan\sqrt{W/E_g}. \quad (7)$$

The function $\Lambda(\Omega)$ is shown in Figure 1 in [17]. Further, we will assume that $E_g/2W \ll 1$, and assume

$$\sqrt{v} = A\pi V^2 = 6\pi V^2/W^{3/2},$$

that

$$f_\pm(\pm E_g/2) = \sqrt{vE_g},$$

$f_{\mp}(\mp E_g/2) = 0$ and $\Lambda(\mp E_g/2) = \pm\sqrt{vE_g}$. It is also easy to show that $df_{\pm}/d\Omega = \pm f_{\pm}(\Omega)/2r_{\pm}(\Omega)$ and

$$\lim_{\Omega\to\Omega_{V,C}} [d\Lambda(\Omega)/d\Omega] = -\sqrt{v} \lim_{\Omega\to\Omega_{V,C}} \left(\frac{1}{r_-(\Omega)} + \frac{1}{r_+(\Omega)}\right), \tag{8}$$

where $\Omega_{V,C} = E_{V,C} - \omega_0$. This value has divergences at $|\Omega| \to E_g/2$.

The resulting band gap is (E_V, E_C) and $\overline{\Lambda}(\mu) = 2\Lambda(\mu)$ for identical sheets (symmetric case). Both situations when the resulting band gap is equal to $(E_{V1(2)}, E_{C1(2)})$ at $E_{g1} < E_{g2}$ $(E_{g2} < E_{g1})$, and situations when these band gaps take values (E_{V1}, E_{C2}) or (E_{V2}, E_{C1}) are possible in case of sheets made of different materials (the asymmetric case). In this case $\overline{\Lambda}(\mu) = \Lambda_1(\mu) + \Lambda_2(\mu)$. Table 1 shows the energy parameters of bulk semiconductors, and Figure 1 shows the values E_V and E_C. The calculation uses data from Table 4.1 provided in [18], the energy of the Dirac point relative to the vacuum was equated to the graphene work function equal to 4.5 eV [19]. It follows from Figure 1, firstly, that $E_C > \varepsilon_D > E_V$ for most semiconductors and band gaps are higher than ε_D only for InAs, InSb, ZnO, CdS and CdSe. Secondly, for all compounds $E_V > -1$ eV, i. e., the edges of the valence bands are ~ 2 eV from the lower Van Hove singularity, whose energy is equal to $-1t \sim -3$ eV [20], where t is the energy of the electron hopping between the nearest neighbors in graphene. The edges of the conduction band E_C of all the considered semiconductors (except ZnO and possibly ZnS and CdS) lie below the upper Van Hove singularity t. (Strictly speaking, the low-energy approximation used in [13,14] works at energies significantly lower than t). Thirdly, the values of the band parameters vary widely (in eV): from 0.18 (InSb) to 3.66 (ZnS), E_C from 0.10 (GaSb) to 2.86 (ZnS), E_V from -1 (AlAs) to 0.39 (InAs). Such large variations in parameters allow, in principle, purposefully selecting encapsulating materials. Note that in the case of native graphene in the limit of weak coupling with sheets, the best materials for the manufacture of the latter are semiconductors with values E_V or E_C, as close as possible to the Dirac point.

Table 1. 3D semiconductors: band gap width E_g, electronic affinity χ and position of the center of the band gap relative to the energy of the graphene Dirac point ω_0 in eV

Crystal	E_g	χ	ω_0
Si	1.11	3.99	−0.05
Ge	0.66	4.14	0.03
AlP	2.45	3.57	−0.30
AlAs	2.15	3.50	−0.08
AlSb	1.63	3.59	0.10
GaP	2.27	3.56	−0.20
GaAs	1.43	3.59	0.20
GaSb	0.70	3.90	0.25
InP	1.34	4.17	−0.34
InAs	0.36	4.89	−0.57
InSb	0.18	4.53	−0.12
ZnO	3.20	4.60	−1.70
ZnS	3.66	3.70	−1.03
ZnSe	2.67	4.00	−0.84
ZnTe	2.25	3.35	0.03
CdS	2.42	4.70	−1.41
CdSe	1.74	4.78	−1.15
CdTe	1.50	4.18	−0.43

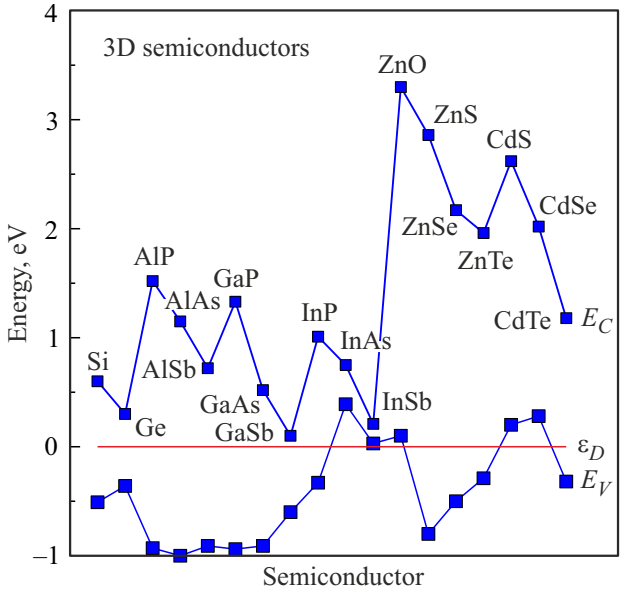

Figure 1. Bulk semiconductors: the energy values of the edges of the zones E_V and E_C for Si, Ge and binary compounds III−V and II−I. The straight line corresponds to the energy of the graphene Dirac point $\varepsilon_D = 0$.

Consider the functions $\sigma^*(\mu)$,

$$L(\mu) = d\ln\sigma^*/d\mu \propto -S^* = -S/(\pi^2 k_B^2 T/3e)$$

and

$$PF^*(\mu) = (\sigma^*)^{-1}(d\sigma^*/d\mu)^2$$

with $|\Omega| \to E_g/2$ in the regime of weak coupling of sheets with graphene $V^2 \ll (E_g/2)^2 \ll \xi^2$. Note that it is this very regime (which can be maintained technologically) that allows preserving the uniqueness of graphene properties, since the carbon monolayer in the limit of strong bonding can be considered as a set of non-interacting adatoms. It is easy to show that the qualitative nature of the dependencies $\sigma^*(\mu)$, $L(\mu)$ and $PF^*(\mu)$ is the same as in Figure 1 in [14], but the conductivity for all energies remains finite. Moreover, this character is universal for the chemical potential located near the Dirac point of graphene.

Using the formula (4) from [14] and the results (6)−(8), we obtain for the symmetric case at $\mu \to E_{V,C} - \omega_0$

$$\sigma^*_{V,C} \propto \sqrt{vE_g}/\gamma, \quad |L_{V,C}| \propto 1 \Big/ \sqrt{E_g(\Omega_{V,C} - \mu)},$$

$$PF^*_{V,C} \propto \sqrt{v/E_g} \Big/ \gamma(\Omega_{V,C} - \mu). \tag{9}$$

Thus, the values $\sigma^*_{V,C}$ are directly proportional to $\sqrt{E_g}$, whereas the values $|L_{V,C}| \propto |S^*_{V,C}|$ and $PF^*_{V,C}$ are inversely proportional to $\sqrt{E_g}$. Therefore, narrow-band semiconductors should be used for sheets to obtain the maximum values of the Seebeck coefficient S and the thermoelectric power factor PF, whereas wide-band semiconductors are of interest in the case of conductivity. Therefore, it is recommended to select intermediate (moderate) values E_g [4]. We also note the papers [7,21,22], which demonstrate that the maximum value of ZT is achieved in narrow-band bulk materials.

Expressions (9) can also be obtained for asymmetric structures by replacing $E_{V,C}$ and E_g with $E^*_{V,C}$ and $E^*_g = E^*_C - E^*_V$ (see [14] for more details). It is clear that the appropriate selection of sheets allows purposefully varying the position of the level μ, at which the maximum TE characteristics of SLG are reached.

3.2. Metal sheets

Let's consider bulk transition metals (3DM) as encapsulating slabs, using the results of [23]. DOS is written in the following form for non-magnetic d-metals

$$\rho_{\rm M}(\omega) = \rho_s(\omega) + \rho_d(\omega),$$

$$\rho_{s(d)}(\omega) = \begin{cases} N_{s(d)}/W_{s(d)}, & |\Omega_{s(d)}| \le W_{s(d)}/2, \\ 0, & |\Omega_{s(d)}| > W_{s(d)}/2, \end{cases} \qquad (10)$$

where $\rho_{s(d)}(\omega)$ is density of states $s(d)$-zones with a width of $W_{s(d)}$, $\Omega_{s(d)} = \omega - \omega_{s(d)}$, $\omega_{s(d)}$ is the energy of the center

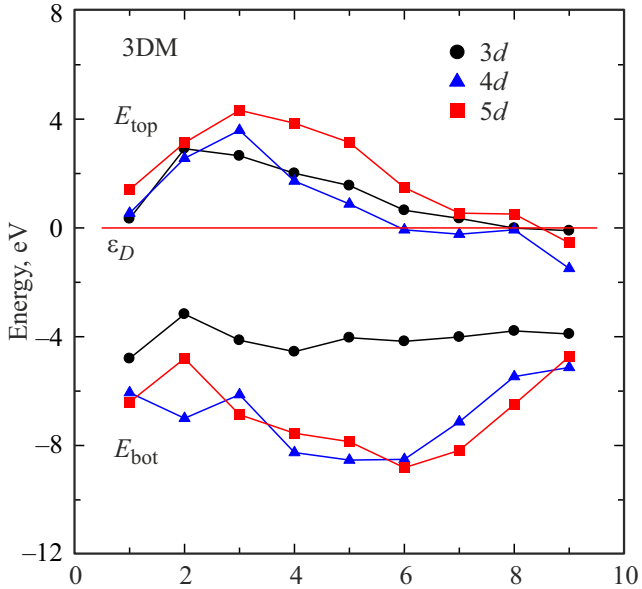

Figure 2. Bulk d-metals: energies of the upper $E_{\rm top}$ and lower $E_{\rm bot}$ edges of the d-zone. 3d-metals: *1* — Sc, *2* — Ti, *3* — V, *4* — Cr, *5* — Mn, *6* — Fe, *7* — Co, *8* — Ni, *9* — Cu; 4d-metals: *1* — Y, *2* — Zr, *3* — Nb, *4* — Mo, *5* — Tc, *6* — Ru, *7* — Rh, *8* — Pd, *9* — Ag; 5d-metals: *1* — Lu, *2* — Hf, *3* — Ta, *4* — W, *5* — Re, *6* — Os, *7* —Ir, *8* — Pt, *9* — Au. The straight line corresponds to the energy of the graphene Dirac point $\varepsilon_D = 0$.

of the $s(d)$-zone, $N_s = 2$, $N_d = 10$ (Friedel model [24,25]). Since $W_s \gg W_d$ (see [25] and the approximation of an infinitely wide s-zone in the Anderson model [26]), we neglect the shift of the electronic states of graphene induced by the s-band, and the broadening of these states is represented as $\gamma_s = 2\pi V_s^2/W_s$, where V_s is the matrix element of the interaction of s-electrons with graphene electrons. The shift of graphene states caused by the d-band is equal to

$$\Lambda_d(\omega) = \frac{\gamma_d}{\pi} \ln \left| \frac{W_d/2 + \Omega_d}{W_d/2 - \Omega_d} \right|, \qquad (11)$$

where the broadening of $\gamma_d = 10\pi V_d^2/W_d$, and V_d is the matrix element of the interaction of d-electrons with graphene electrons. The ratio of the parameters γ_d and γ_s was discussed in [27]. Further, we assume that $\gamma_d \gg \gamma_s \gg \gamma$. The total broadening in the area of s-zone is equal to $\Gamma_s = 2\gamma_s + \gamma$ for a symmetrical encapsulated structure, it is equal to $\Gamma_d = 2\gamma_d + 2\gamma_s + \gamma$ in the area of d-zone. It bears reminding that the broadening of the levels is associated with their temporal attenuation: $\tau_{s,d} \sim \hbar/\Gamma_{s,d}$. From (11) we have $d\Lambda(\omega)/d\omega = (\gamma_d W_d/\pi)/[(W_d/2)^2 - \Omega_d^2]$. Using the formula (4) from [14] for the case when the level $|\mu_d| \equiv |\mu - \omega_d| \to W_d/2$ and lies outside the d-zone, we obtain

$$\sigma^* \propto (\gamma_d/\gamma_s) \ln(W_d/|\mu_d - W_d/2|).$$

$$|L| \propto W_d/|\mu_d - W_d/2| \ln(W_d/|\mu_d - W_d/2|),$$

$$PF^* \propto (\gamma_d/\gamma_s)[W_d^2/(\mu_d - W_d/2)^2] \ln(W_d/|\mu_d - W_d/2|). \qquad (12)$$

The factor $\gamma_d/\gamma_s \gg 1$ should be replaced with 1 if $|\mu_d|$ is located in the d-zone. It follows that all the considered thermoelectric characteristics turn to infinity if $\mu_d \equiv \mu - \omega_d \to W_d/2$.

3DM energy characteristics, including the energies in the midpoints of d-band ω_d obtained from data provided in [24,25,28], are listed in Table 2, and Figure 2 shows the upper $E_{\rm top}$ and the lower $E_{\rm bot}$ boundaries of these zones. Figure 2 suggests that (under the condition of low doping of graphene in the mode of weak coupling with sheets) the maximum values of TE characteristics can be achieved for sheets made of Sc, Y, Lu and the last elements of the d-rows. In this regard, it should be noted that copper and gold are widely used for the manufacture of contact pads in Van der Waals heterostructures [29].

The issue of bilayer graphene (BLG) encapsulated with 3d sheets is considered in *Appendix*.

4. 2D sheets

4.1. Semiconductor sheets

The DOS of graphene-like (GLC) binary semiconductor structures $A_N B_{8-N}$ can be represented as

$$\rho_{\rm AB}(\overline{\Omega}) = \begin{cases} \frac{2|\overline{\Omega}|}{\overline{\xi}^2}, & \sqrt{\overline{\xi}^2 + \Delta^2} \ge |\overline{\Omega}| \ge |\Delta|, \\ 0, & |\overline{\Omega}| < |\Delta|, \ |\overline{\Omega}| > \sqrt{\overline{\xi}^2 + \Delta^2}. \end{cases} \qquad (13)$$

Table 2. 3D transition metals: ϕ_M work function, width of d-band and position of the center of the band relative to the graphene Dirac point ω_d in eV

3*d* 4*d* 5*d*	Sc Y Lu	Ti Zr Hf	V Nb Ta	Cr Mo W	Mn Tc Re	Fe Ru Os	Co Rh Ir	Ni Pd Pt	Cu Ag Au
ϕ_M	3.50 3.10 3.30	4.10 3.84 3.53	4.11 4.00 4.20	4.38 4.29 4.50	3.35 4.70 4.95	3.70 4.71 4.95	4.16 4.65 5.27	4.60 4.73 5.32	4.00 4.00 4.45
W_d	5.13 6.59 7.81	6.08 8.37 9.56	6.77 9.72 11.12	6.56 9.98 11.44	5.60 9.42 11.02	4.82 8.44 10.31	4.35 6.89 8.71	3.78 5.40 7.00	2.80 3.63 5.28
$-\omega_d$	2.23 2.76 2.50	0.13 0.41 2.22	−0.74 −1.27 0.49	−1.93 −3.27 1.85	−1.24 −3.83 2.36	−1.76 −4.29 3.67	−1.83 −3.68 3.82	−1.90 −2.77 2.99	−1.50 −3.31 2.09

Here $\overline{\Omega} = \omega - \overline{\varepsilon}$, where $\overline{\varepsilon} = (\varepsilon_a + \varepsilon_b)/2$ is the middle of the gap with width $2\Delta = \varepsilon_a - \varepsilon_b$, $\varepsilon_{a(b)}$ is energy of p-orbital of the atom A(B), $\overline{\xi} = \sqrt{2\pi\sqrt{3}\overline{t}}$, $\overline{t}$ is the transition energy between p_z-orbitals of the nearest atoms A and B [30]. The corresponding broadening function is $\Gamma(\overline{\Omega}) = \pi\overline{V}^2\rho_{\mathrm{AB}}(\overline{\Omega})$, and the shift function is

$$\Lambda(\overline{\Omega}) = \frac{2\overline{V}^2}{\overline{\xi}^2}\,\overline{\Omega}\ln\left|\frac{\overline{\Omega}^2 - \Delta^2}{\overline{\Omega}^2 - \Delta^2 - \overline{\xi}^2}\right|, \qquad (14)$$

where $\overline{V}$ is matrix element of the GLCis graphene interaction. As shown in [14], the maximum values of static conductivity and thermoelectric characteristics are achieved under the condition $\overline{\mu}^2 \equiv (\mu - \overline{\varepsilon})^2 \to \Delta^2$. We obtain the following for symmetric structures

$$\sigma^*_{\pm\Delta} \propto \overline{\Lambda}_\Delta/\gamma, \quad |L_{\pm\Delta}| \propto C_\Delta/\overline{\Lambda}_\Delta, \quad PF^*_{\pm\Delta} \propto C^2_\Delta/\gamma\overline{\Lambda}_\Delta, \quad (15)$$

where

$$\overline{\Lambda}_\Delta \approx (4\overline{V}^2\Delta/\overline{\xi}^2)\ln[\overline{\xi}^2/(\Delta^2 - \overline{\mu}^2)],$$
$$C_\Delta \approx 4\overline{V}^2\Delta^2/\overline{\xi}^2(\Delta^2 - \overline{\mu}^2),$$

which assumes that the chemical potential is located inside the GLC gap. It should be noted that the general dependencies $\sigma^*(\mu)$, $L(\mu)$ and $PF^*(\mu)$ are analyzed in [14] and the model symmetric structure h-BN/Gr/h-BN is considered in detail, for which $\overline{\varepsilon} = 0$, since the Gr h-BN work functions coincide. Turning to other 2D A_NB_{8-N} compounds, it is necessary firstly to note the most well studied two-dimensional silicon carbide and aluminum and gallium nitrides, information about which is contained respectively in [31,32]. Data on the width of the gaps (band gaps) are provided in these papers, but, unfortunately, there is no information about electronic affinity, which prevents from estimating $\overline{\varepsilon}$ values. Therefore, here we will consider 2D transition metal dichalcagenides (TMD), studied much more thoroughly than 2D A_NB_{8-N} (see, for example, reviews [33,34]). Table 3 presents the data obtained by numerical calculations from the first principles [35]. The maximum effects of increasing thermoelectric characteristics for undoped SLG, weakly bound to the sheets, will be observed for MoS_2 when the chemical potential approaches the bottom of the conduction band and for $MoTe_2$ and WTe_2 — to the ceilings of the valence bands.

Based on the results obtained using the strong coupling approximation [36–38] and $\mathbf{k}\cdot\mathbf{p}$-method [39], for rough estimates, we represent TMD DOS as $\rho(\overline{\Omega}) = \overline{\rho} = \mathrm{const}$ at $|\overline{\Omega}| \geq E_g/2$ and $\rho(\overline{\Omega}) = 0$ at $|\overline{\Omega}| < E_g/2$ (Haldane–Anderson model [40]). Then the shift function

$$\Lambda(\overline{\Omega}) = \overline{\rho}\overline{V}^2\ln|(\overline{\Omega} - E_g/2)/(\overline{\Omega} + E_g/2)|$$

and

$$d\Lambda(\overline{\Omega})/d\overline{\Omega} = \overline{\rho}\overline{V}^2E_g/[\overline{\Omega}^2 - (E_g/2)^2].$$

We obtain the following if $\overline{\mu}^2 \equiv (\mu - \overline{\varepsilon})^2 \to (E_g/2)^2$ and μ remain in the TMD band gap in the symmetric structure

$$\sigma^* \propto \overline{\rho}\overline{V}^2\ln[E_g/(E_g/2 - |\overline{\mu}|)]/\gamma,$$
$$|L| \propto E_g/[(E_g/2)^2 - \overline{\mu}^2]\ln[E_g/(E_g/2 - |\overline{\mu}|)],$$
$$PF^* \propto \overline{\rho}\overline{V}^2E_g^2/\gamma[(E_g/2)^2 - \overline{\mu}^2]^2\ln[E_g/(E_g/2 - |\overline{\mu}|)]. \qquad (16)$$

If μ is outside the TMD band gap, then in expressions (16) it is necessary to change the sign of the differences $(E_g/2 - |\overline{\mu}|)$ and $[(E_g/2)^2 - \overline{\mu}^2]$, and γ replace with $\gamma + 2\overline{\Gamma}$ (where $\overline{\Gamma} = \pi\overline{\rho}\overline{V}^2$ is broadening of graphene levels due to interaction with the TDM plate) and $\overline{\Gamma} \gg \gamma$. Thus, MoS_2 appears to be the most promising sheet material (from the considered TDM series).

4.2. Metal sheets

The intensive search for new materials, which began immediately after the start of graphene studies, led to the publication of articles on 2D metals (2DM) [41–44], in which various variants of DFT (density functional theory)

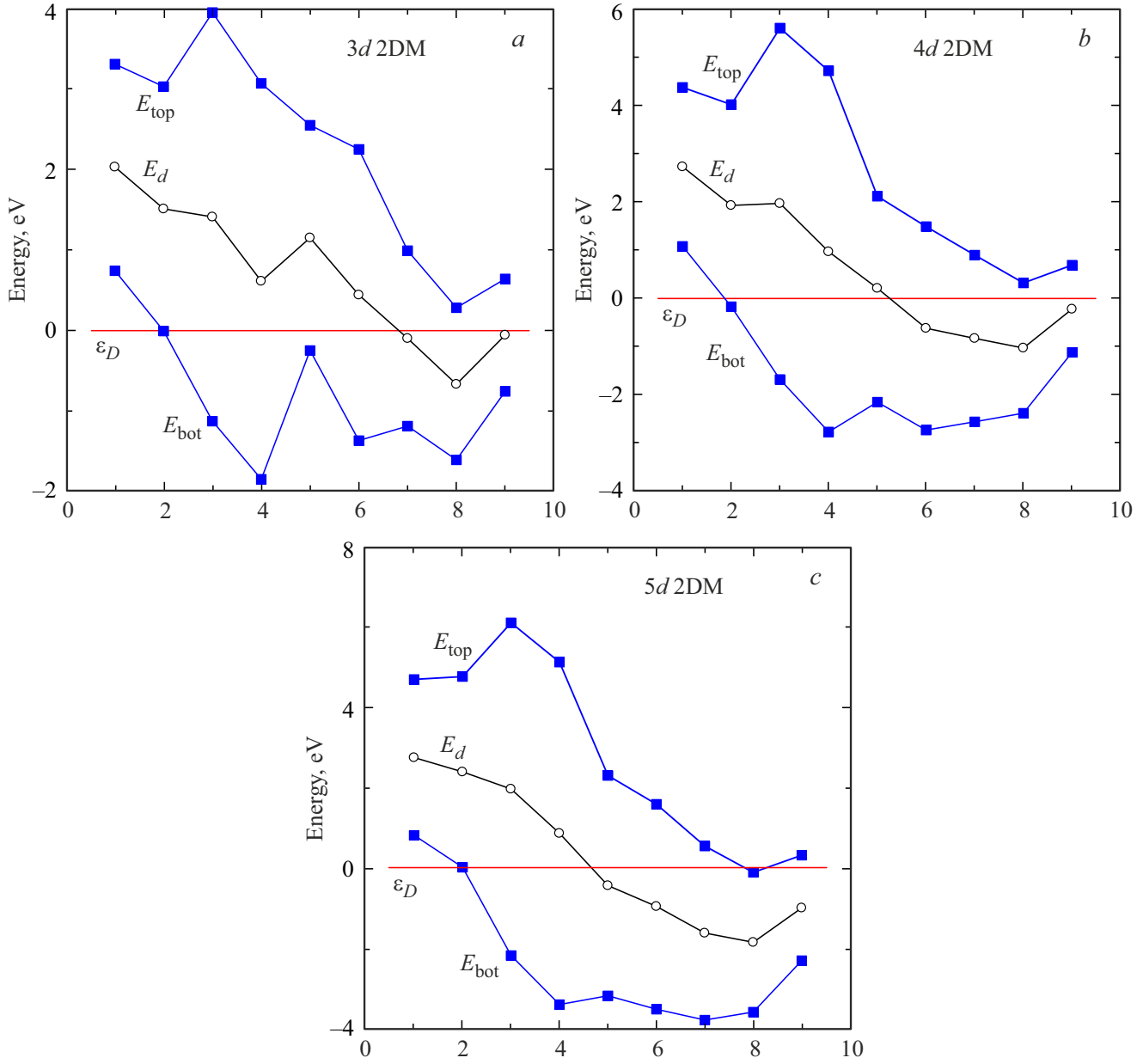

Figure 3. Two-dimensional d-metals: energies of the midpoint E_d (light circles), upperE_{top} and lower E_{bot} edges (dark squares) d-zones. *a* — 3d-metals: *1* — Sc, *2* — Ti, *3* — V, *4* — Cr, *5* — Mn, *6* — Fe, *7* — Co, *8* — Ni, *9* — Cu; *b* — 4d-metals: *1* — Y, *2* — Zr, *3* — Nb, *4* — Mo, *5* — Tc, *6* — Ru, *7* — Rh, *8* — Pd, *9* — Ag; *c* — 5d-metals: *1* — Lu, *2* — Hf, *3* — Ta, *4* — W, *5* — Re, *6* — Os, *7* — Ir, *8* — Pt, *9* — Au. The straight line corresponds to the energy of the graphene Dirac point $\varepsilon_D = 0$.

were used for calculations. Unfortunately, there is no data either on the widths of the d-zones W_d, or on the transition metal work functions in [41–44]. It was demonstrated, however, that the 2DM constant lattices are almost identical to the 3DM constant lattices. It follows that the values of the transition energies t_{3DM} and t_{2DM} are also close. Since $W_d \propto z$ in the strong coupling approximation, where z is the number of nearest neighbors, it is possible to write $W_d(2DM) \approx \eta W_d(3DM)$, where $\eta = z_{2DM}/z_{3DM} < 1$. It is this circumstance that was used in [45] for the model description of the zone characteristics of the transition 2DM. As for the 2DM work functions, they were equated to

Table 3. 2D semiconductor transition metal dichalcagenides: band gap E_g, electronic affinity χ and position of the center of the band gap $\overline{\varepsilon}$ and its edges $\overline{E}_C$ and $\overline{B}_V$ relative to the energy of the graphene Dirac point in eV

TMD	E_g	χ	$\overline{\varepsilon}$	$\overline{E}_C$	$\overline{E}_V$
MoS_2	1.59	4.28	−0.58	0.22	−1.37
$MoSe_2$	1.33	3.91	−0.08	0.59	−0.74
$MoTe_2$	0.94	3.81	0.22	0.69	−0.25
WS_2	1.55	3.93	−0.21	0.57	−1.08
WSe_2	1.25	3.61	0.26	0.89	−0.36
WTe_2	0.74	3.67	0.46	0.83	0.09

the 3DM work functions in [45]. It is appropriate to emphasize here that, according to the handbook [28], even for well-studied refractory metals, the spread of values of ϕ_{M} is very significant. The values of the midpoints E_d and edges E_{top} and E_{bot} of the 2DM d-zones obtained in this way are shown in Figure 3. For undoped graphene in the mode of weak bond with sheets, the most promising materials for thermoelectric applications are the finite elements of the d-rows, the edges of the d-zones of which are close to the Dirac point, and the initial elements for which the bottom of the d-zone is located near ε_D.

It is natural to use the same Friedel model to describe 2DM DOS as for 3DM in section 3.2. Therefore, the extreme values of the functions σ^*, $|L|$ and PF^* are described by expressions (12). It should be noted that $W_d(\mathrm{2DM}) < W_d(\mathrm{3DM})$, whereas the ratios (γ_d/γ_s) for 3DM and 2DM, according to our estimates, are approximately equal.

The question of BLG encapsulated with 2D sheets is discussed in *Appendix*.

5. Conclusion

The dependence of the static conductivity σ, the Seebeck coefficient S and the thermoelectric power factor $PF = \sigma S^2$ of graphene on the nature and dimension of the sheets of the encapsulated structure and the position of the chemical potential μ is investigated in this paper. 3D and 2D semiconductors ($A_N B_{8-N}$ and TMD) and transition metals are considered as the materials of the sheets. Graphene was considered in a low-energy approximation, simple models were used to describe the densities of the states of the sheets.

It is shown for 3D semiconductor slabs that the maximum values of S and σS^2 are achieved when μ, being in the area of overlap of the band gaps of sheets 1 and 2, i.e. in the interval $E_g^* = E_C^* - E_V^*$, tends to E_V^* or E_C^*. In this case, σ takes the maximum finite value proportional to $(E_g^*)^{1/2}$, whereas $|S|$, $PF \to \infty$ as $(E_g^* \delta_{V,C})^{-1/2}$ and $(E_g^* \delta_{V,C})^{-1/2} \delta_{V,C}^{-1/2}$, where $\delta_{V,C} = |E_{V,C}^* - \mu|$. It is shown for 2D semiconductor TMDs that in a symmetric structure, when the chemical potential is found inside the band gap E_g, we have

$$\sigma^* \propto \ln(E_g/\overline{\delta}), \quad |L| \propto (E_g/w) \ln^{-1}(E_g/\overline{\delta})$$

and

$$PF^* \propto (E_g/w)^2 \ln^{-1}(E_g/\overline{\delta}),$$

where $\overline{\delta} = E_g/2 - |\mu|$ and $w = (E_g/2)^2 - \overline{\mu}^2$. Since the logarithm is a weakly varying function, the similarity of the results for 3D and 2D sheets is obvious. It is interesting to note that it is possible to change the width of the resulting band gap by placing graphene encapsulated with 2D semiconductor sheets in a vertical electrostatic field. For a symmetrical structure, for example, we have a constriction E_g of the form $E_g' = E_g - eFl$, where F is field strength, l is distance between 2D sheets. The value can be either reduced or increased in the case of an asymmetric structure. In this case, the Dirac point experiences a shift of $\Delta\varepsilon_D = eFl/2$. The positions of the extremes σ, S and PF can be shifted in this way.

The maximum values of the considered characteristics for volumetric and two-dimensional sheets made of d-metals are achieved for the chemical potential located near the boundaries of the d-zone. In this case we have

$$\sigma^* \propto \ln(W_d/\delta_d), \quad |L| \propto (W_d/\delta_d) \ln^{-1}(W_d/\delta_d)$$

and

$$PF^* \propto (W_d/\delta_d)^2 \ln^{-1}(W_d/\delta_d),$$

where $\delta_d = |\mu_d - W_d/2|$. Thus, the difference between 3D and 2D sheets is reduced to differences in the widths of d-zones: $W_d(\mathrm{2DM}) < W_d(\mathrm{3DM})$. It should be emphasized that the divergences of the functions $\sigma(\mu)$, $S(\mu)$ and $PF(\mu)$ considered by us are not related to the topological features of the encapsulated structures, but to the coarseness of the DOS models adopted for the sheets. The divergences turn into extremes of finite height when more complex models are used. The same effect will take into account not only the shift of the electronic states of graphene induced by the sheets, which is considered in this paper, but also their broadening. We also emphasize that the results obtained here for SLG are also valid for gapless silicene, germanene and stanene and, under certain conditions, for BLG (see *Appendix*).

The presence of a substrate (as well as sheets) can cause the appearance of relatively narrow slits (on the order of tenths of eV) in the electronic spectrum of graphene in the vicinity of the Dirac point [46,47]. It is shown in [48] that when the chemical potential overlaps with the boundaries of the gap induced by the sheets, extremes of these characteristics will be observed.

In conclusion, it should be noted that shortcomings of Mott's formula are often noted in the theoretical literature (see, for example, [48,49] and the references given there). Nevertheless, almost all experimental results are discussed on the basis of this formula. Moreover, the Mott formula is also used in calculations [1–13], including for the study of TE temperature dependencies. Since in this paper we use the Drude model for graphene conductivity (excluding electron-electron and electron-phonon interactions) and strive only for qualitative (at best, semi-quantitative) results, we believe that the use of the Mott formula in describing a rather complex structure of encapsulated graphene is fully justified.

Appendix

Here we will consider the thermoelectric properties of encapsulated bilayer graphene, or BLG. The electronic spectrum of free BLG has the following form [50,51]

$$\varepsilon_{\pm}^{\pm}(\mathbf{k}) = \pm t_{\perp}/2 \pm \sqrt{(t_{\perp}/2)^2 + t^2 f^2(\mathbf{k})}, \qquad (\Pi.1)$$

where

$$f(\mathbf{k}) = \sqrt{3 + 2\cos(k_y a\sqrt{3}) + 4\cos(k_y a\sqrt{3}/2)\cos(3k_x a/2)},$$

t and $t_\perp$ are electron jump energies between the nearest carbon atoms in the monolayer (located at a distance of a from each other) and the nearest atoms in the upper and lower layers of BLG, respectively $(t_\perp/t \sim 0.1)$ $\mathbf{k} = (k_x, k_y)$ is the wave vector of an electron in a monolayer lying in the plane (x, y), the energy of the Dirac point ε_D is taken as zero, the subscripts correspond to the signs before the first term on the right side of the expression (p.1), superscripts correspond to signs before the radical. It is easy to see that the expression $\varepsilon_\pm^\pm(\mathbf{k}) \mp t_\perp/2$ for four BLG zones exactly coincides with the law of dispersion for two free GLC zones of the form $E_\pm(\mathbf{k}) - \varepsilon = \sqrt{\Delta^2 + t^2 f^2(\mathbf{k})}$, where $\varepsilon = (\varepsilon_a + \varepsilon_b)/2$, $\Delta = (\varepsilon_a - \varepsilon_b)/2$ and $\varepsilon_{a(b)}$ are the energies of the p-orbitals of atoms A(B) [52]. In the low-energy approximation, the corresponding DOS is equal to

$$\rho_\pm^\pm(\Omega_\pm) = \begin{cases} \frac{2|\Omega_\pm|}{\xi^2}, & R \geq |\Omega_\pm| \geq t_\perp/2, \\ 0, & |\Omega_\pm| > t_\perp/2, \ |\Omega_\pm| > R, \end{cases} \qquad (\Pi.2)$$

where $R = \sqrt{\xi^2 + t_\perp^2/4}$. Since $t \sim 3\,\text{eV}$, $t_\perp \sim 0.4\,\text{eV}$, then at $|\omega| \gg t_\perp/2$ DOS BLG (p.2) switches to double DOS SLG, where $\rho_{\text{SLG}}(\omega) = 2|\omega|/\xi^2$ at $|\omega| \leq \xi$ and $\rho_{\text{SLG}}(\omega) > 0$ at $|\omega| > \xi$. It follows that for $|E_V^*|$, $|E_C^*| \gg t_\perp/2$ and $\mu \to E_V^*, E_C^*$, all conclusions of clause 3.1 made for SLG with $3d$ sheets are valid for BLG. Similarly, for $|\Delta| \gg t_\perp/2$ and $\overline{\mu} \to \Delta$, the conclusions of clauses 3.2 for SLG with $2d$ sheets correspond to the present case. Further, since $W_d \gg t_\perp$ (for both $3d$ and $2d$), then at $|\mu_d| \to W_d/2$ all the conclusions of clauses 3.2 and 4.2 can be attributed to BLG as well. Thus, the expressions (9), (12), (15) and (16) are also valid for BLG if the characteristics of sheet DOS occur at energies whose values are much greater than $t_\perp/2$. In cases where the DOS characteristics of the encapsulating layers have energies of the order $t_\perp/2$, it is necessary to calculate the static conductivity (for example, according to the scheme of work [13,14]), followed by the Seebeck coefficient and the thermoelectric power factor BLG.

Encapsulated BLG (as well as encapsulated SLG) can be considered as an element of a superlattice, where the layers of BLG (SLG) alternate with the sheets. In this regard, we note that the interest in BLG as an element of superlattices has a ten-year history [53–59]. At the same time, it is logical to use the scheme of operation [60], which is close to the scheme used in this paper.

Conflict of interest

The authors declare that they have no conflict of interest.

References

[1] A.M. Dehkordi, M. Zebarjad, J. He, T.M. Tritt. Mater. Sci. Engin. R: Reports, **97**, 1 (2015).

[2] Y. Xia, J. Park, F. Zhou, V. Ozolins. Phys. Rev. Appl., **11**, 024017 (2019).

[3] E.B. Isaacs, C. Wolverton. Phys. Rev. Mater., **3**, 015403 (2019).

[4] S. Wei, C. Wang, S. Fan, G. Gao. J. Appl. Phys., **127**, 155103 (2020).

[5] D. Li, Y. Gong, Y. Chen, J. Lin, Q. Khan, Y. Zhang, Y. Li, H. Zhang, H. Xie. Nano-Micro Lett., **12**, 36 (2020).

[6] H. Usui. K. Kuroki. J. Appl. Phys., **121**, 165101 (2017).

[7] E.H. Hasdeo, L.P.A. Krisna, M.Y. Hanna, B.E. Gunara, N.T. Hung, A.R.T. Nugraha. J. Appl. Phys., **126**, 035109 (2019).

[8] Y. Xia, J. Park, V. Ozolins, C. Wolverton. Phys. Rev. B, **100**, 201401(R) (2019).

[9] J.M. Adhidewata, A.R.T. Nugraha, E.H. Hasdeo, P. Estell, B.E. Gunara. arXiv: 2107.06826.

[10] A. Darmawan, E. Suprayoga, A.R.T. Nugraha, A.A. AlShaikhi. arXiv: 2107.10603.

[11] K.L. Grosse, M.-H. Bae, F. Lian, E. Pop, W.P. King. Nature Nanotechnol., **6**, 287 (2011).

[12] J. Duan, X. Wang, X. Lai, G. Li, K. Watanabe, T. Taniguchi, M. Zebarjadi, E.Y. Andrei. PNAS, **113**, 14272 (2016).

[13] Z.Z. Alisultanov. Low Temp. Phys., **39**, 592 (2013).

[14] S.Yu. Davydov. Phys. Solid State, 65, 635 (2023).

[15] S.Yu. Davydov. Techn. Phys. Lett., **47**, 649 (2021).

[16] C. Persson, U. Lidefelt. Materials Science Forum, **264–268**, 275 (1998).

[17] S.Yu. Davydov. Techn. Phys., **59**, 624 (2014).

[18] F. Bechstedt, R. Enderline. *Poverkhnosti i granitcy razdela poluprovodnikov* (M., Mir, 1990) ch. 4 (in Russian).

[19] S. Mammadov, J. Ristein, J. Krone, C. Raidel, M. Wanke, V. Wiesmann, F. Speck, T. Seyller. 2D Mater., **4**, 015043 (2017).

[20] A.H. Castro Nero, F. Guinea, N.M.R. Peres, K.S. Novoselov, A.K. Geim. Rev. Mod. Phys., **81**, 109 (2009).

[21] J.O. Sofo, G.D. Mahan. Phys. Rev. B, **49**, 4565 (1994).

[22] Z.M. Gibbs, H.S. Kim, H. Wang, G.J. Snyder. Appl. Phys. Lett., **106**, 022112 (2015).

[23] S.Yu. Davydov. FTT, **64** (6), 817 (2021) (in Russian).

[24] V.Y. Irkhin, Y.P. Irkhin. *Elektronnaya struktura, fizicheskie svojstva i korrelyacionnye effekty v d- i f-metallah i ikh soedineniyakh* (Ekatirenburg, UrO RAN, 2004) ch. 2. (in Russian).

[25] U. Harrison. *Elektronnaya struktura i svojstva tverdykh tel* (M., Mir, 1983) ch. 20. (in Russian).

[26] C. Kittel. *Kvantovaya teoriya tverdykh tel* (M., Nauka, 1967) ch. 18. (in Russian).

[27] S.Yu. Davydov, O.V. Posrednik. Tech. Phys. Lett., **47** (11), 37 (2021). (in Russian).

[28] V.S. Fomenko. *Emissionnye svojstva materialov* (Kiev, Nauk. dumka, 1981).

[29] I.V. Antonova. Semiconductors, **50**, 66 (2016).

[30] S.Yu. Davydov. Semiconductors, **51**, 217 (2017).

[31] S.Yu. Davydov. Semiconductors, **54**, 523 (2020).

[32] S.Yu. Davydov. Phys. Solid State, **62**, 1085 (2020).

[33] A. Chaves, J.G. Azadani, H. Alsalman, D.R. da Costa, R. Frisenda, A.J. Chaves, S.H. Song, Y.D. Kim, D. He, J. Zhou, A. Castellanos-Gomez, F.M. Peeters, Z. Liu, C.L. Hinkle, S.-H. Oh, P.D. Ye, S.J. Koester, Y.H. Lee, Ph. Avouris, X. Wang, T. Low. 2D Mater. Appl., **4**, 29 (2020).

[34] Y. Jing, B. Liu, X. Zhu, F. Ouyang, J. Sun, Y. Zhou. Nanophotonics, **9**, 1675 (2020).

[35] J. Kang, S. Tongay, J. Zhou, J. Li, J. Wu. Appl. Phys. Lett., **102**, 012111 (2013).
[36] J.Á. Silva-Guillén, P. San-Jose, R. Roldán. Appl. Sci., **6**, 284 (2016).
[37] A.C. Dias, F. Qu, D.L. Azevedo, J. Fu. Phys. Rev. B, **98**, 075202 (2018).
[38] S.K. Pandey, R. Das, P. Mahadevan. ACS Omega, **5**, 15169 (2020).
[39] S. Aas, C. Bulutaya. J. Appl. Phys., **126**, 115701 (2019).
[40] F.D.M. Haldane, P.W. Anderspn. Phys. Rev. B, **13**, 2553 (1976).
[41] J. Nevalaita, P. Koskinen. Phys. Rev. B, **97**, 035411 (2018).
[42] J. Nevalaita, P. Koskinen. AIP Advances, **10**, 065327 (2020).
[43] S. Ono. Phys. Rev. B, **102**, 166424 (2020).
[44] T. Wang, M. Park, Q. Yu, J. Zhang, Y. Yang. Materials Today Advances, **8**, 100092 (2020).
[45] S.Yu. Davydov. Phys. Solid State, **55**, 1536 (2013).
[46] S. Kim, J. Ihm, H.J. Choi, Y.-W. Son. Phys. Rev. Lett., **100**, 176802 (2008).
[47] T. Jayasekera, S. Xu, K.W. Kim, B. Nardell. Phys. Rev. B, **84**, 035442 (2011).
[48] A.A. Varlamov, A.V. Kavokin, I.A. Luk'yanchuk, S.G. Sharapov. Phys.-Uspekhi, **55**, 1146 (2012).
[49] J.M. Buhmann, M. Sigrist. Phys. Rev. B, **88**, 115128 (2013).
[50] M.I. Katsnelson. *Graphene* (N.Y., Cambridge University Press, 2012).
[51] E. McCann, M. Koshino. Rep. Progr. Phys., **76**, 056503 (2013).
[52] S.Yu. Davydov. Phys. Solid State, **58**, 804 (2016).
[53] M. Barbier, P. Vasilopoulos, F.M. Peeters. Phil. Trans. R. Soc., Math. Phys. Engin. Sci., **368**, 5499 (2011).
[54] M. Killi, S. Wu, A. Paramekanti. Phys. Rev. Lett., **107**, 086801 (2011).
[55] T.P. Kaloni, Y.C. Cheng, U. Schwingenschlögl. J. Mater. Chem., **22**, 919 (2012).
[56] F. Sattari, E. Faizabadi. Inter. J. Mod. Phys. B, **27**, 1350024 (2013).
[57] C.H. Pham, T.T. Nguyen, V.L. Nguyen. J. Appl. Phys., **116**, 123707 (2014).
[58] L. Azadi, S. Shojaei. J. Comput. Electron., **20**, 1248 (2021).
[59] S.A.A. Ghorashi, A. Dunbrack, J. Sun, X. Du, J. Cano. arXiv: 2206.13501.
[60] S.Yu. Davydov. Phys. Solid State, **64**, 1792 (2022).

Translated by Ego Translating